GENETICS, 2023, 224(1), iyad051
https://doi.org/10.1093/genetics/iyad051
Advance Access Publication Date: 27 March 2023
Investigation

Regulation of the hypertonic stress response by the 3′ mRNA cleavage and polyadenylation complex

Sarel J. Urso,[1,2] Anson Sathaseevan,[3] W. Brent Derry,[3] Todd Lamitina[1,2,4,*]

[1]Graduate Program in Cell Biology and Molecular Physiology, University of Pittsburgh Medical Center, Pittsburgh, PA 15261, USA
[2]Department of Cell Biology, University of Pittsburgh School of Medicine, Pittsburgh, PA 15261, USA
[3]Developmental and Stem Cell Biology Program, Peter Gilgan Centre for Research and Learning, The Hospital for Sick Children, Toronto, ON M5G 0A4, Canada
[4]Division of Child Neurology, Department of Pediatrics, Children's Hospital of Pittsburgh, University of Pittsburgh Medical Center, Pittsburgh, PA 15224, USA

*Corresponding author: Email: stl52@pitt.edu

Abstract

Maintenance of osmotic homeostasis is one of the most aggressively defended homeostatic set points in physiology. One major mechanism of osmotic homeostasis involves the upregulation of proteins that catalyze the accumulation of solutes called organic osmolytes. To better understand how osmolyte accumulation proteins are regulated, we conducted a forward genetic screen in *Caenorhabditis elegans* for mutants with no induction of osmolyte biosynthesis gene expression (Nio mutants). The *nio-3* mutant encoded a missense mutation in *cpf-2*/CstF64, while the *nio-7* mutant encoded a missense mutation in *symk-1*/Symplekin. Both *cpf-2* and *symk-1* are nuclear components of the highly conserved 3′ mRNA cleavage and polyadenylation complex. *cpf-2* and *symk-1* block the hypertonic induction of *gpdh-1* and other osmotically induced mRNAs, suggesting they act at the transcriptional level. We generated a functional auxin-inducible degron (AID) allele for *symk-1* and found that acute, post-developmental degradation in the intestine and hypodermis was sufficient to cause the Nio phenotype. *symk-1* and *cpf-2* exhibit genetic interactions that strongly suggest they function through alterations in 3′ mRNA cleavage and/or alternative polyadenylation. Consistent with this hypothesis, we find that inhibition of several other components of the mRNA cleavage complex also cause a Nio phenotype. *cpf-2* and *symk-1* specifically affect the osmotic stress response since heat shock-induced upregulation of a *hsp-16.2::GFP* reporter is normal in these mutants. Our data suggest a model in which alternative polyadenylation of 1 or more mRNAs is essential to regulate the hypertonic stress response.

Keywords: osmotic stress, *Caenorhabditis elegans*, screen, ENU, alternative polyadenylation, mutagenesis

Introduction

mRNA processing plays a key role in the response to diverse types of environmental stress. For example, post-transcriptional splicing of the *xbp-1* mRNA by activated IRE1 endonuclease is the key step in activation of the endoplasmic reticulum (ER) stress response (Calfon *et al.* 2002). In the DNA damage response, localized mRNA splicing plays a key role in the active repair of double strand breaks (Shanbhag *et al.* 2010; Pederiva *et al.* 2016). In the heat shock response, hsp-70 mRNA undergoes alternative polyadenylation (APA), resulting in a shortened 3′ UTR, the function of which is unknown (Tranter *et al.* 2011; Kraynik *et al.* 2015). Likewise, 3′ UTR lengthening through selection of more distal polyadenylation sites (PASs) is a common feature of ribotoxic stress (Hollerer *et al.* 2016). Recently, 3′ mRNA cleavage components from transcriptionally active genomic loci were found to undergo hyperosmotic stress-induced phase separation, which was associated with a global impairment of transcriptional termination (Jalihal *et al.* 2020). Whether or not 3′ mRNA cleavage or other types of mRNA processing play a more direct functional role in the regulation of the hyperosmotic stress response is unknown.

In eukaryotes, the 3′ ends of ~30–60% of all mRNAs are cleaved and polyadenylated at more than 1 PAS, which results in mRNAs with different 3′ ends (Steber *et al.* 2019; Yuan *et al.* 2021). Much like alternative splicing, APA also leads to the diversification of mRNA transcripts through 2 distinct mechanisms. First, 3′ UTR APA gives rise to mRNAs with different length 3′ UTRs, which can provide isoform-specific binding sites for mRNA regulators such as microRNAs (miRNAs) and RNA-binding proteins (Mayr and Bartel 2009). Second, upstream region APA (UR-APA) can include alternative exons that, when translated, give rise to proteins with unique sequences and/or domains (Alt *et al.* 1980). The 3′ mRNA end processing complex is composed of ~85 proteins that regulate mRNA cleavage, polyadenylation, and APA (Shi *et al.* 2009). Biochemical and structural features of the core complex of ~20 protein are relatively well described (Pancevac *et al.* 2010; Clerici *et al.* 2017, 2018), and new sequencing and bioinformatics approaches are enabling the identification of mRNA targets of APA (Ha *et al.* 2018; Wang *et al.* 2018). While APA is associated with aspects of cellular physiology, such as cellular stress responses (Chang *et al.* 2018; Zheng *et al.* 2018), the physiological roles of 3′ mRNA cleavage/APA are poorly understood, largely because genetic null alleles of most 3′ mRNA cleavage components

Received: January 20, 2023. **Accepted:** March 10, 2023

are lethal, although some important exceptions do exist (Subramanian *et al.* 2021).

In *Caenorhabditis elegans*, hypertonic stress activates a gene expression program that restores cell volume and protects against hypertonicity-induced macromolecular damage (Rohlfing *et al.* 2010). Like all cells and organisms, *C. elegans* uses solutes called organic osmolytes to restore volume and provide protection (Lamitina *et al.* 2004, 2006; Burkewitz *et al.* 2012). The major *C. elegans* osmolyte is glycerol, which is rapidly accumulated following exposure to hypertonicity, in part through the upregulation of the glycerol-3-phosphate dehydrogenase *gpdh-1* (Lamitina *et al.* 2004). Genetic screens for regulators of *gpdh-1* expression have identified many positive and negative regulators of this stress response pathway (Lamitina *et al.* 2006; Rohlfing *et al.* 2010, 2011; Urso *et al.* 2020; Wimberly and Choe 2022). However, it is not known whether components of the 3′ mRNA cleavage complex play a functional role in the regulation of the hypertonic stress response.

Using unbiased forward genetic screening for mutants that exhibit no induction of *gpdh-1* expression in response to hypertonicity, we identified viable hypomorphic alleles of 2 3′ mRNA cleavage complex genes, *cpf-2* and *symk-1*. *cpf-2* and *symk-1* physiologically regulate the transcriptional induction of multiple hypertonicity induced mRNAs through their activity in the hypodermis and intestine. CPF-2 and SYMK-1 proteins colocalize within the nucleus of all cells and form subnuclear puncta in response to hypertonicity. Both *symk-1* and *cpf-2* mutants do not significantly alter general mRNA polyadenylation but instead exhibit phenotypes consistent with inhibition of APA. Consistent with this hypothesis, inhibition of several other 3′ mRNA cleavage complex genes also blocks hypertonic induction of *gpdh-1* transcription. *cpf-2* and *symk-1* are not required for the transcriptional induction of a heat shock inducible GFP reporter, suggesting that their roles in regulating stress response pathways may be specific. Our findings reveal a physiological role for the 3′ mRNA cleavage complex in the hypertonic stress response and provide new genetic tools that should facilitate the in vivo study of this essential mRNA regulatory mechanism in developmental and tissue-specific contexts.

Materials and methods

C. elegans strains and culture

Strains were cultured on standard NGM media with *Escherichia coli* OP50 bacteria at 20°C unless otherwise noted. Hypertonicity was induced by increased plate NaCl concentration to either 250 or 600 mM NaCl. For the auxin-induced degradation experiments, we included 0.5–1.0 mM naphthaleneacetic acid (K-NAA) in the NGM media prior to pouring plates. A list of strains used in this study can be found in Table 1.

Genetic methods

L4 stage *drIs4* animals (P_0) were mutagenized in 0.6 mM *N*-ethyl-*N*-nitrosourea (ENU) diluted in M9 for 4 h at 20°C, and Nio mutants were isolated as previously described (Urso *et al.* 2020). Backcrossing of both *nio-3(dr16)* and *nio-7(dr23)* to the wild-type *drIs4* strain showed that both mutants were recessive. *Trans*-heterozygotes between *dr16* and *dr23* exhibited complementation. SNPs in both *dr16* and *dr23* were identified using whole-genome resequencing and a Galaxy workflow (Urso *et al.* 2020). Candidate genes were tested using gene-specific RNAi in the *drIs4* background. RNAi was performed as described previously (Urso *et al.* 2020).

Table 1. *Caenorhabditis elegans* strains.

Strain	Genotype
OG119	*drIs4 (gpdh-1p::GFP; col-12p::dsRed2)*
OG975	*nio-3/cpf-2(dr16); drIs4*
OG996	*nio-7/symk-1(dr23); drIs4*
OG1137	*symk-1(dr88); drIs4*
OG1165	*cpf-2(dr99); drIs4*
OG1200	*kin-20(dr116)*
OG1202	*kin-20(dr118); symk-1(dr88)*
OG1207	*cpf-2(dr121); lin-15(n765ts)*
OG1209	*cpf-2(dr99); kin-20(dr122)*
OG1224	*wrdSi23* (eft-3p:TIR-1:F2A: mTAG BFP2:AID* NLS: tbb3′ UTR); *drIs4; symk-1(dr127)* [*symk-1::AID*::GFP*]
OG1226	*reSi2* (col-10p:TIR-1:F2A: mTAG BFP2:AID* NLS: tbb3′UTR); *drIs4; symk-1 (dr129)* [AID* GFP CRISPR into *symk-1*]
OG1227	*reSi12* (ges-1p:TIR-1:F2A: mTAG BFP2:AID* NLS: tbb3′UTR); *drIs4; symk-1 (dr130)* [AID* GFP CRISPR into *symk-1*]
OG1241	*cpSi171* [vha-8p::TIR1::F2A::mTagBFP2::AID*::NLS::tbb-2 3′ UTR]; *drIs4; symk-1(dr142)* [AID* mNeonGreen CRISPR into *symk-1*]
OG1142	*cpf-2(dr92)* (TagRFP CRISPR at N-terminus of CPF-2)
OG1144	*ogt-1(dr84); cpf-2(dr92)*
OG1194	*symk-1(dr111)* (GFP CRISPR just before NLS)
OG1195	*cpf-2(dr92); symk-1(dr112)* (GFP CRISPR just before NLS)
OG1203	*cpf-2(dr99); gpIs1*
OG1204	*symk-1(dr88); gpIs1*
OG1205	*cpf-2(dr92 dr119); symk-1(dr112)* (TagRFP::cpf-2 with G42E and symk-1::GFP)

COPAS Biosort acquisition and analysis

Day 1 adults from a synchronized egg lay or hypochlorite preparation were seeded on 50 or 250 mM NaCl OP50 or the indicated RNAi NGM plates. After 18 h, the GFP and RFP fluorescence intensities, time-of-flight (TOF), and optical extinction (EXT) of each animal were acquired with the COPAS Biosort. Events in which the RFP intensity of adult animals (TOF > 400) was <20 (dead worms or other objects) were excluded from the analysis. The GFP fluorescence intensity of each animal was normalized to its RFP fluorescence intensity. To determine the fold induction of GFP for each animal, each GFP/RFP was divided by the average GFP/RFP of that strain exposed to 50 mM NaCl.

CRISPR/Cas9 genomic editing

For CRISPR editing, we injected purified and assembled Cas9/gRNA/tracrRNA complexes with the purified repair template (all from IDT) and the *rol-6* marker plasmid into the germlines of day 1 adult hermaphrodites. Editing protocols primarily followed Ghanta and Mello (2020) with some modifications. We found that the high concentrations of nucleic acids frequently led to precipitation of Cas9 complexes and needle clogging during injection. Reducing the input levels of gRNA and tracer RNA to 20 ng/μl and repair templates to 25 ng/μl (oligo repair) or 10 ng/μl (PCR-based repair templates) prevented needle clogging and led to similar numbers of editing events. Overall, 10–20 P0s were injected and 2–3 plates with >10 rollers were selected for screening. Since CRISPR editing appears to occur primarily in the distal germline while transgene formation occurs primarily in the proximal germline, we screened 24 non-Rol F1 animals that were younger than the Rol animals for editing events using edit-specific PCR approaches. We isolated homozygous edit-positive animals from 2–3 independent heterozygous P0s. All edits were verified by DNA sequencing. A list of all guide RNAs, repair template oligos/primers, and genotyping primers can be found in Table 2.

Table 2. Primers used in this study.

Primer	Primer sequence	Notes
OG592	TGCAGAGATTCCAGGAAACCAGG	gpdh-1 qPCR sense
OG593	CCCTTTTGTAGCTTGCCACGGAG	gpdh-1 qPCR antisense
OG596	GTAATGGATCCATCGCCAACAACTT	hmit-1.1 qPCR sense
OG597	GGTTAAGCCCGCGTATAGCCAAA	hmit-1.1 qPCR antisense
OG606	ggaggatatggaagaggatatggagga	nlp-29 qPCR sense
OG607	ccgtatcctccgtacattccacgtc	nlp-29 qPCR antisense
OG1342	tacctgttccatggccaacacttgtc	GFP qPCR sense
OG1343	CTTTCCTGTACATAACCTTCGGGC	GFP qPCR antisense
OG1720	ccgaagacacgattcgctccatt	cpf-2(dr16) sequencing fwr primer
OG1721	aacttcggcggtttgaatgtctg	cpf-2(dr16) sequencing rev primer
OG1722	cgataaagaagctgcggagatgt	symk-1(dr23) sequencing fwr primer
OG1723	gttcgagtagccttgatattgtg	symk-1(dr23) sequencing rev primer
OG1753	attttattctttccaattaaaatactgaaaaaaaggatccaggcagaaatgtgtt gtcgatcaaaatggttcacgatcggg	ssDNA repair template for CRISPR conversion of WT to cpf-2/nio-3(dr16) Gly–>Glu
OG1756	gtggagcaaggttgatgtatcagaaattagttgtctggcttacaacgaggttt tgggaagattgtactccatttgaagaaaagttgat	ssDNA repair template for CRISPR conversion of symk-1 WT to dr23
OG1757	tccggctgacgactagattc	gRNA symk-1
OG1780	CAGGTTGAAAAATGATGTCC	gRNA for N-term CRISPR insertion of TagRFP into cpf-2
OG1781	aatttattcattttcaatttccaggttgaaaaatggtatccaagggagaagagttgatt	sense primer for TagRFP-cpf-2 N-term fusion (SP9 at 5′ end)
OG1782	TTGCCCACTCCGGATGATTTGTATCCTCCGGACATGGCGCC GAATTCAGATCTCCTAGG	antisense primer for TagRFP-cpf-2 N-term fusion (SP9 at 5′ end)
OG1783	gggtggagctagaggcaacgaatatg	tRFP-cpf-2 genotyping N-term
OG1784	GGATTCCTTGGGTGTGGTTGATGAAG	tRFP-cpf-2 genotyping N-term
OG1785	gcgggcgcgcagttttcgcaagtgtg	tRFP-cpf-2 genotyping N-term
OG1786	CGGGATCCGTACATGAAGGAGGTGGC	tRFP-cpf-2 genotyping N-term
OG1787	cacctaccgttccaagaagccagcc	tRFP-cpf-2 genotyping C-term
OG1788	CGAATTGCAACTTCGGCGGTTTGAATG	tRFP-cpf-2 genotyping C-term
OG1789	CAAGATGCCAGGAGTCTACTACGTC	tRFP-cpf-2 genotyping C-term
OG1790	GGAAATTCAATAAATCCGTATCCC	tRFP-cpf-2 genotyping C-term
OG1791	CGATCAAAATGGTTCACGAT	gRNA for CRISPR conversion of cpf-2 to dr16
OG1938	cttaattgtaataatttcagcgagaaaatcaaagaagagttgcatgatatgagt aaaggagaagaact	sense primer for symk-1-GFP template (SP9 modified at 5′)
OG1939	AGTCGCTTATCTCGTTCACGATTTTCTCGTTCTTTTTTGT ATAGTTCATCCATGC	antisense primer for symk-1-GFP template (SP9 modified at 5′)
OG1940	ttcgaatcgttcgtcgcaaatc	symk-1 GFP screening primer
OG1941	TTCCTTTCCACTTTCGCGAGTTCG	symk-1-GFP screening primer
OG1942	GAAGATGTATCAACAATCGGATCG	symk-1 GFP screening primer
OG1943	GCGAGTTCGTTCCTTTTCTCTTTCC	symk-1-GFP screening primer
OG1944	GGGTAAGTTTTCCGTATGTTGCA	symk-1-GFP screening primer
OG1937	TTTCAGCGAGAAAATCAAAG	gRNA for symk-1 GFP
OG1953	aacatcaacatatcgcatat	kin-20 gRNA
OG1954	ttggactagcgaaacgctatcgtgatagcaaacattaacatatcgcatatcgc gaaaataagaatctaactggaactgcaagatacgc	kin-20(ox423) repair template with mutation
OG1955	gccggataacttttgatgggtct	kin-20 outer primer (sense)
OG1956	TGCAACTTCAAAAACATACCAATTC	kin-20 outer primer (antisense)
OG1957	gatgggtcttggaaagcgagg	kin-20 inner primer (sense)
OG1958	CCTCGATGAGTATTTATACTGGCG	kin-20 inner primer (antisense)
OG1959	GCATAAGGTGTTCACCGGGCACCAC	gpdh-1 3′ UTR for polyA length assay
OG1960	GTTCATTCAAAATCAAAAATTGTACA	gpdh-1 3′ UTR for polyA length assay
OG1983	AACCATGAAGATCAAGATCATCGC	act-2 3′ UTR for polyA length assay
OG1984	CGGGGTGTGAAAATCCGTAAGGC	act-2 3′ UTR for polyA length assay
OG1993	GTCTTCCTCCAGGGACCACGATCTG	rpl-18 sense—polyA length (spans exons 4/5)
OG1994	GACACATTTTTATTCGGCATGATTCG	rpl-18 3′ UTR antisense—polyA length
OG1995	CAGATGAAGAAGGTTCTCTGCCTCTC	rpl-1 sense—polyA length (spans exons 2/3)
OG1996	CAACAATGTTTATTGAATAACAAAG	rpl-1 antisense—polyA length
OG1997	GGTTCATGATCAGGTTCTCGATGGAG	col-144 sense—polyA length (spans exons 1/2)
OG1998	GCAAACTTTATAATTGTGTGTTTGGAG	col-144 antisense—polyA length
OG1999	CAAGACGGACAACGTGGATCCGGAGC	col-144 sense—polyA length (in exon 2/use in case longer product does not work)
OG2000	GTCGCCGTTATCTCGGTGTGCGTCACTCTTCC	col-117 sense polyA length (spans exons 1/2)
OG2001	GTTGAATTTCTCATAACATTTAACGG	col-117 antisense—polyA length
OG2002	CCAAACGGAAACCCAGGAGCCCCAG	col-117 sense—polyA length (in exon 2/use in case longer product does not work)
OG2003	GGTTGAGGAAGCTGAGGAACTCGCCAAC	unc-54 sense—polyA length (spans exons 8/9)
OG2004	GTGTACACAGAACATTGTGTAGATTTTGGG	unc-54 antisense—polyA length
OG2005	CTCTTGCCCCATCAACCATGAAGATCAAG	act-3 sense—polyA length (spans exons 2/3)
OG2006	GATGGTCTTTTTGAATGGTCTCATGATCG	act-3 antisense—polyA length
OG2016	cttaattgtaataatttcagcgagaaaatcaaagaagagttgcatgatgg tggcggtggatcgggaggaggagg	sense primer for amplifying GFP-AID* with symk-1 homology (SP9 at 5′ end)
	AGTCGCTTATCTCGTTCACGATTTTCTCGTTCTTTGCCT CCGGACGATGCTCCTGAGGCTC	antisense primer for amplifying GFP-AID* with symk-1 homology (SP9 at 5′ end)

Hypertonic adaptation assay

This assay was previously described, with the modification that adaptation in the present work occurred at 250 mM NaCl (Urso *et al.* 2020). Briefly, day 1 adult animals were placed on NGM plates (3–5 plates containing 10 animals each) containing either 50 mM NaCl (unadapted) or 250 mM NaCl (adapted) for 24 h. Animals from each set were then moved to 600 mM NaCl plates, and motility (defined as the ability to move at least half a body length) was quantified for each animal.

mRNA isolation, cDNA synthesis, qPCR, and polyA tail analysis

Day 1 animals were plated on 50 or 250 mM NaCl OP50 NGM plates for 24 h. After 24 h, 35 animals were picked into 50-µl Trizol for mRNA isolation. RNA isolation followed a combined Trizol/RNeasy column purification method as previously described (Rohlfing *et al.* 2010). cDNA was synthesized from 1-µg total RNA using the SuperScript VILO Master Mix. SYBR Green master mix, 2.5-ng RNA, and the primers listed in Table 2 were used for each quantitative PCR (qPCR) reaction. qPCR reactions were carried out using a BioRad CFX qPCR machine. *act-2* primers were used as a control for all qPCR reactions. At least 3 biological replicates of each qPCR reaction were carried with 3 technical replicates per biological replicate. qPCR data were analyzed through ΔΔCt analysis with all samples normalized to *act-2*. polyA tail length analysis was performed using the Poly(A) Tail-Length Assay Kit (Thermofisher).

*Symk-1-AID** alleles and auxin-induced degradation experiments

*symk-1AID*GFP* or *symk-1-AID*mNeonGreen* cassettes were PCR amplified from previously described plasmids (Ashley *et al.* 2021) and used as the repair substrate for CRISPR/Cas9 injections into *TIR1;drIs4* strains. TIR1 strains were previously described (Ashley *et al.* 2021). AID* alleles of *symk-1* recapitulated the *symk-1* null phenotype (100% emb/larval lethal) when gravid adults expressing TIR1 globally were placed on plates containing either 0.5 or 1.0 mM K-NAA. For tissue-specific Nio experiments, AID* homozygotes eggs were placed onto NGM plates containing 0.5 or 1 mM KAA (Sigma). L4 stage animals were picked to new 1 mM auxin plates and aged for 24 h. Day 1 adults were placed on either 50 mM NaCl NGM/auxin or 250 mM NaCl NGM/auxin plates for 18–24 h. For temporal experiments, day 1 adult *symk-1-AID** was placed on 0.5 mM K-NAA for 4 h prior to transfer. Animals were then imaged, and the GFP and RFP signals from the *drIs4* reporter were quantified on a COPAS Biosort.

Microscopy

For whole worm images, worms were anesthetized (10 mM levamisole) and manually arrayed on agar plates for fluorescence microscopy. Images were collected on a Leica MZ16FA stereo dissecting scope with a DFC345 FX camera (Leica Microsystems, Wetzlar, Germany). Images within an experiment were collected using the same exposure and magnification settings.

kin-20 and *lin-15* suppression assays

The *ox423* allele of *kin-20* was CRISPR edited into WT, *cpf-2(dr99)*, or *symk-1(dr88)*. Verified *kin-20* homozygotes in each background were placed on a clean NGM plate as a day 1 adult. Thirty seconds of movement was video captured using a Leica M205 microscope and DFC camera at 15 frames per second. These data were analyzed for multiple kinetic and kinematic parameters using WormLab (MBF Biosciences).

For *lin-15* suppression, *cpf-2(dr99)* and *symk-1(dr88)* heterozygous males were crossed into *lin-15(n765ts)* at the permissive temperature (16°C) using standard genetic crossing and genotyping methods. For unknown reasons, the *symk-1(dr88)* allele was synthetic lethal with *lin-15(n765ts)*, preventing further analysis. Animals were analyzed for the presence of a multivulval (Muv) phenotype at the restrictive temperature (20°C).

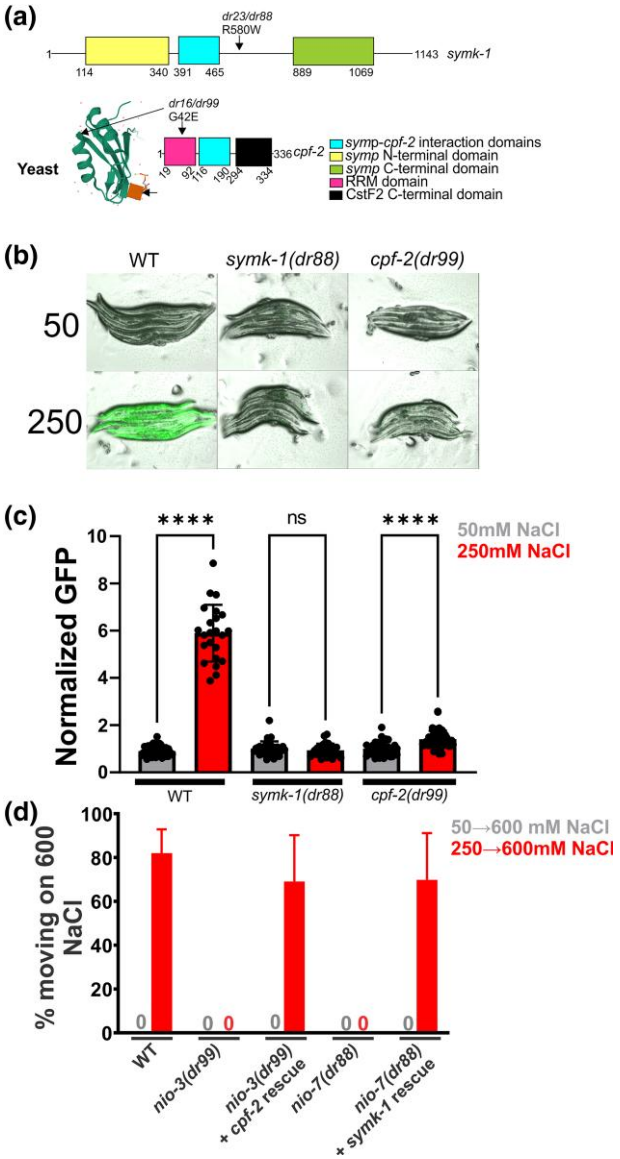

Fig. 1. *nio-3* and *nio-7* are caused by missense mutations in the polyadenylation complex genes *cpf-2* and *symk-1*. a) Protein domains found in SYMK-1 and CPF-2. The location of each missense mutation is indicated. For *cpf-2*, we used the available crystal structure of the APA complex to map the location of the conserved G42 residue on the yeast homolog of *cpf-2*, Rna15 (Pancevac *et al.* 2010). b) Overlayed transmitted light and GFP images of CRISPR-engineered animals carrying missense Nio alleles of either *symk-1* or *cpf-2* exposed to either 50 or 250 mM NaCl for 18 h. c) COPAS quantification of animals imaged in b. Bar graphs show the mean ± SD, with individual data points overlayed. d) Hypertonic adaptation of CRISPR Nio alleles with or without a genomic DNA rescue transgene. Data are the mean ± SD of 4–5 independent replicates of 10–20 worms per replicate.

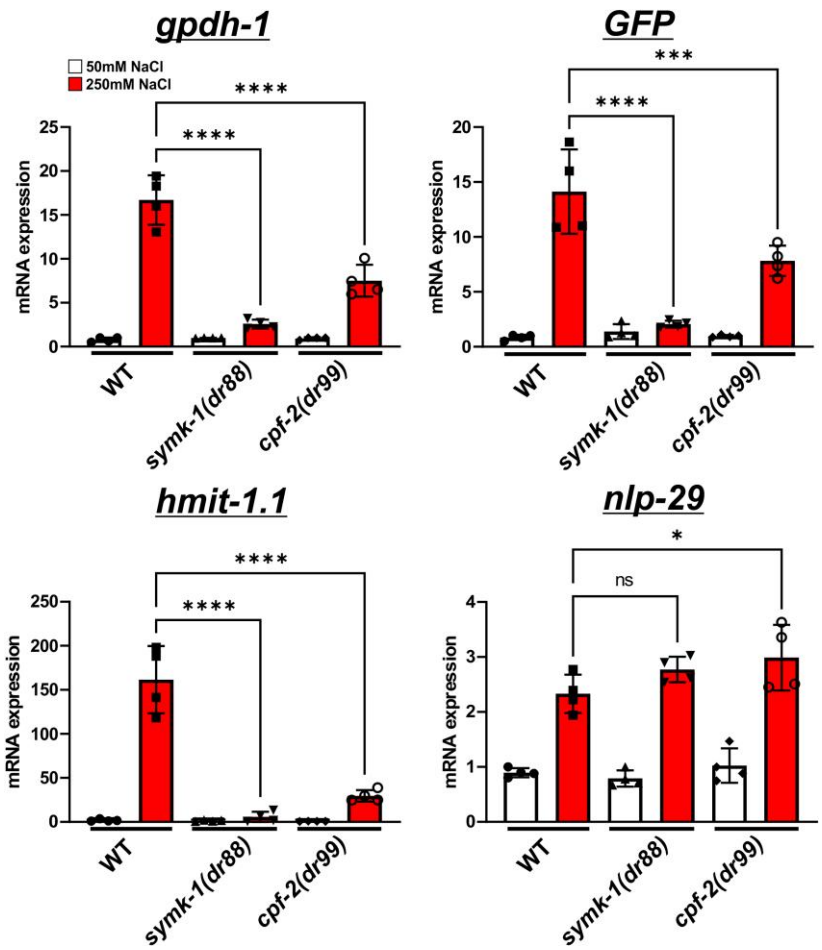

Fig. 2. *cpf-2* and *symk-1* are required for hypertonic stress induced mRNA expression. qPCR of the *gpdh-1*, *gfp* (from the *drIs4* reporter), *hmit-1.1*, and *nlp-29* mRNAs in wild-type, *symk-1(dr88)*, and *cpf-2(dr99)* young adult animals exposed to 50 or 250 mM NaCl NGM. Data are the mean ± SD of 4 independent biological replicates. Individual data points are plotted. $^{****}P < 0.0001$; $^{***}P < 0.001$; $^{*}P < 0.05$; ns $P > 0.05$; 1-way ANOVA with Šidák multiple comparisons test.

Statistical analysis

Comparisons of means were analyzed with either a 2-tailed Student's *t*-test (2 groups) or ANOVA (3 or more groups) using the Dunnett's, Šidák, or Tukey's post-test analysis as indicated in GraphPad Prism 9 (GraphPad Software, Inc., La Jolla, CA, USA). *P*-values of <0.05 were considered significant.

Results

An ENU screen for mutants that inhibit osmosensitive gene expression identify missense alleles in the 3′ mRNA cleavage complex genes *cpf-2* and *symk-1*

In a forward genetic screen for mutants with no induction of the osmolyte biosynthetic transcriptional reporter *gpdh-1p::gfp* reporter (Nio muants), we identified *nio-3(dr16)* and *nio-7(dr23)*. Mapping, complementation testing, and whole-genome sequencing revealed that *dr16* caused a G42E missense mutation in the *cpf-2* gene while *dr23* caused a R580W missense mutation in the *symk-1* gene (Fig. 1a). Both alleles were genetically recessive and segregated Nio animals from heterozygous hermaphrodites close to expected single gene Mendelian ratios (*dr16*–24/111, 21.6%; *dr23*–22/145, 15.2%). *cpf-2* and *symk-1* encode 2 proteins that are core components of the 3′ mRNA cleavage and polyadenylation complex and are known to interact in mammalian cells (Ruepp *et al.* 2011). This complex recognizes polyadenylation signals in the mRNA and directs mRNA cleavage and transcriptional termination through a multisubunit protein complex (Shi *et al.* 2009). Several additional experiments show that these nonnull mutations in *cpf-2* and *symk-1* are the basis for the Nio phenotype. First, post-embryonic RNAi of both *cpf-2* and *symk-1* also caused a Nio phenotype (Supplementary Fig. 1). Second, extrachromosomal arrays carrying either fosmids or genomic DNA PCR products encompassing either the *cpf-2* and *symk-1* loci rescue *dr16* and *dr23* accordingly (Supplementary Fig. 2). Third, CRISPR-engineered alleles of *dr16* and *dr23* that recreated each missense mutation in a nonmutagenized *drIs4* background also blocked hypertonic induction of *gpdh-1p::GFP* (Fig. 1b and c) and eliminated the ability to adapt to normally lethal hypertonic environments (Fig. 1d). Notably, null or strong loss-of-function alleles of both *cpf-2* and *symk-1* are embryonic/larval lethal (Steber *et al.* 2019), whereas the Nio alleles are viable and fertile under isotonic conditions. Taken together, these data show that *nio-3(dr16)* and *nio-7(dr23)* are caused by nonnull hypomorphic alleles in *cpf-2* and *symk-1*.

cpf-2 and *symk-1* Nio alleles block hypertonic upregulation of specific mRNA transcripts

The Nio screen utilized the *drIs4* reporter strain to identify mutants with defective transcriptional responses to hypertonic

stress. To determine if these alleles also affected endogenous mRNAs, we performed qPCR on several genes previously shown to be upregulated by hypertonicity (Rohlfing *et al.* 2010). Hypertonic upregulation of endogenous *gpdh-1* mRNA, as well as another hypertonicity upregulated gene *hmit-1.1* and the transgene derived *gfp* mRNA, was strongly attenuated in both *cpf-2(dr99)* and *symk-1(dr88)* (Fig. 2). However, upregulation of *nlp-29*, an antimicrobial peptide previously shown to be induced by infection, wounding, and hypertonicity (Pujol *et al.* 2008), continued to be upregulated to wild-type levels in *cpf-2(dr99)* and *symk-1(dr88)*. Therefore, *cpf-2* and *symk-1* are required to upregulate some but not all hypertonicity responsive mRNAs.

cpf-2 and *symk-1* function post-developmentally in the hypodermis and intestine to regulate hypertonic upregulation of *gpdh-1*

gpdh-1 is upregulated by hypertonic stress in the intestine and the hypodermis (Lamitina *et al.* 2004, 2006). If *cpf-2* and *symk-1* function cell autonomously, then they should also be required in the intestine and hypodermis to upregulate *gpdh-1* in response to hypertonicity. To test this hypothesis, we generated auxin-inducible degradation (AID*) alleles for both *cpf-2* and *symk-1* using CRISPR/Cas9 methods. The *AID*-GFP-cpf-2* allele was sick and exhibited low fecundity, suggesting the presence of nonspecific *cpf-2* degradation and was not studied further. However, the *symk-1::GFP::AID** allele exhibited qualitatively normal growth and fertility in the absence of auxin, suggesting this allele is functional. We generated homozygous *symk-1::GFP::AID** alleles in genetic backgrounds expressing the TIR1 E3 ligase in all cells, hypodermis, intestine, or hypodermis and intestine (Ashley *et al.* 2021). While *symk-1::GFP::AID** animals expressing global TIR1 robustly expressed nuclear GFP in all somatic and germline cells in the absence of auxin, exposure of animals to 0.5 mM auxin led to loss of the GFP signal in all tissues within 3–4 h (Supplementary Fig. 3). Additionally, 100% of the progeny derived from L4 animals exposed to 0.5 mM auxin paired with global expression of TIR1 were embryonic or larval lethal, suggesting that auxin-induced depletion of *symk-1* mimics the *symk-1* null phenotype.

Next, we examined induction of the *gpdh-1p::GFP* reporter in each TIR1 strain in the absence of auxin. GFP expression was induced in the intestine and hypodermis to similar levels as wild type (Supplementary Fig. 4). When animals were exposed to auxin starting as L1s, hypertonic induction of GFP was inhibited in the global TIR1 strain as much as in the *symk-1(dr88)* allele (Fig. 3a and b). Hypodermal depletion of *symk-1* led to strong inhibition of GFP induction by hypertonicity, although there was still statistically significant induction. Intestinal depletion of *symk-1* had a minor effect on GFP induction, which also remained statistically significant. However, simultaneous depletion of *symk-1* in both the intestine and hypodermis resulted in a complete block in hypertonicity *induced gpdh-1::GFP* expression (Fig. 3b). We next utilized the *symk-1 AID** allele and hypodermal/intestinal TIR1 to examine the temporal requirements for *symk-1* in the activation of *gpdh-1*. Exposure to auxin for 4 h in day 1 adult animals immediately prior to exposure to hypertonicity was sufficient to block *gpdh-1p::GFP* expression (Fig. 3c). Taken together, these data show that *symk-1* functions cell autonomously in the hypodermis and intestine to regulate hypertonic *gpdh-1* induction. Additionally, they show that *symk-1* has a post-developmental physiological role in this process.

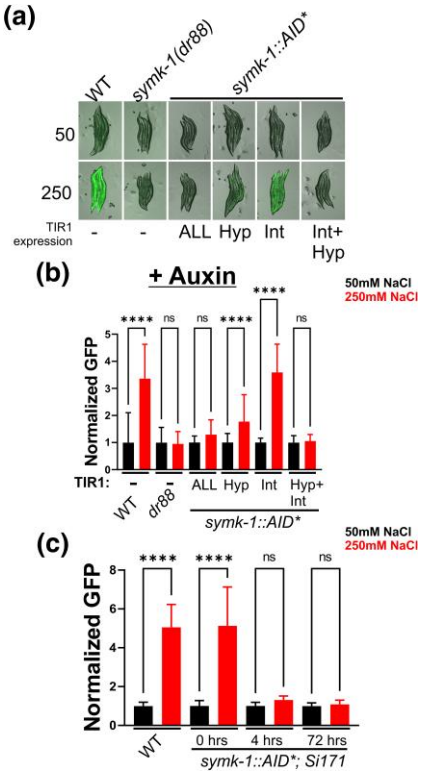

Fig. 3. *symk-1* is required post-developmentally in the hypodermis and intestine for the Nio phenotype. a) Overlayed GFP and transmitted light images of *gpdh-1p::gfp* expression following 24 h of exposure to 50 or 250 mM NaCl. Animals express TIR1 in the indicated tissues and were exposed to 1 mM K-NAA from the L1 stage. b) COPAS Biosort quantification of GFP expression from animals shown in a. Data shown are mean ± SD. $N = 41$–89 animals per sample. ****$P < 0.0001$; ns $P > 0.05$; 1-way ANOVA with Dunn's multiple comparison test. c) COPAS Biosort quantification of animals with TIR1 expression in the hypodermis and intestine (*cpSi171*) exposed to 1 mM K-NAA for 0, 4, or 72 h prior to exposure to 50 or 250 mM NaCl. Data shown are mean ± SD $N = 35$–61 animals per sample. **** $P < 0.0001$; ns $P > 0.05$.

cpf-2 and *symk-1* colocalize to subnuclear foci following exposure to hypertonic stress

If *cpf-2* and *symk-1* interact within the 3′ mRNA cleavage complex in *C. elegans* as they do in mammalian cells (Ruepp *et al.* 2011), we predicted that they should exhibit spatial colocalization. Indeed, GFP and RFP alleles of endogenous *cpf-2* and *symk-1*, respectively, showed that both proteins are expressed ubiquitously (Fig. 4a–c), exhibit colocalization in the nucleoplasm, and are excluded from the nucleolus (Fig. 4d–f). Following exposure to hypertonicity, both proteins formed subnuclear puncta that exhibited complete colocalization (Fig. 4g–i). In the same screen that isolated *cpf-2* and *symk-1*, we also identified mutations in the O-GlcNAc transferase homolog *ogt-1*, suggesting that these 3 proteins could be components of the same complex that regulates the hypertonic stress response. However, our data were inconsistent with this model. We found that the CPF-2 and SYMK-1 puncta were distinct from previously reported OGT-1 puncta induced by hypertonic stress (Supplementary Fig. 5) (Urso *et al.* 2020). Hypertonicity-induced CPF-2/SYMK-1 puncta were most apparent in the hypodermis while no puncta were observed in germline nuclei (Fig. 4g–i). We considered the possibility that the missense alleles isolated in our Nio screen may disrupt protein abundance, nuclear localization, colocalization, and/or foci formation in response to hypertonic stress. To test this hypothesis, we introduced the

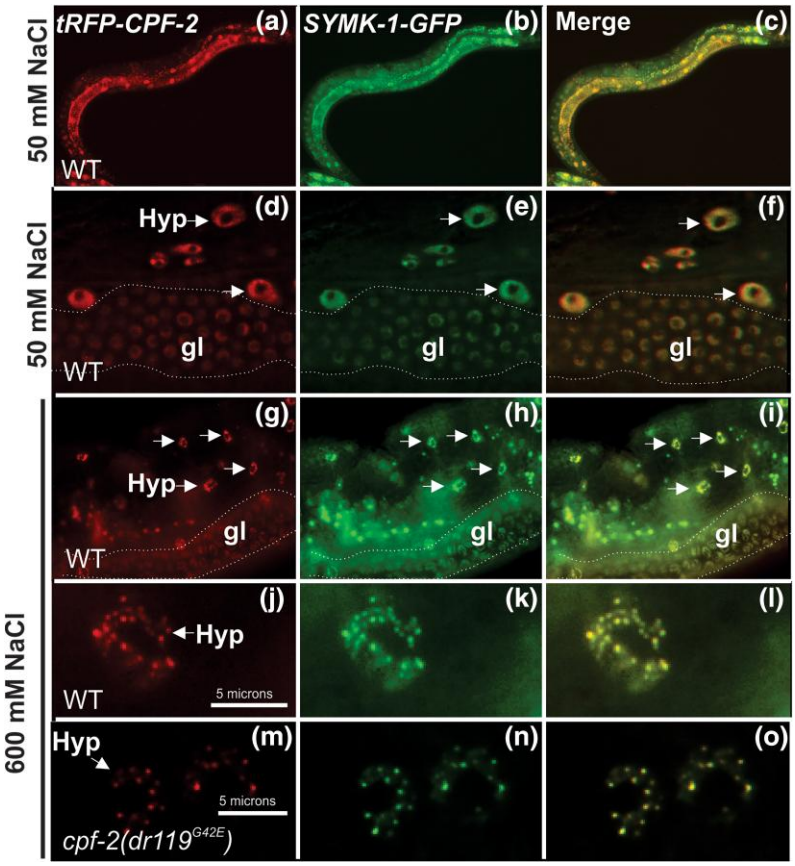

Fig. 4. CPF-2 and SYMK-1 proteins colocalize into subnuclear puncta following exposure to hypertonic stress. Expression of CRISPR/Cas9-tagged alleles of *Tag-RFP::cpf-2* (a) *symk-1::gfp* (b), and the merged image (c). (d–f) Higher resolution images of hypodermal (hyp arrows) and germline (gl) nuclei revealing the nonnucleolar nucleoplasmic concentration of tagged SYMK-1 and CPF-2 proteins. Dotted lines delineate the boundaries of the germline. (g–i) Exposure of animals to 600 mM NaCl for 1 h leads to reorganization of SYMK-1 and CPF-2 localization, primarily in the hypodermis. (j–l) Higher resolution of hypodermal nuclei with SYMK-1 and CPF-2 subnuclear foci. (m–o) higher resolution of hypodermal nuclei with SYMK-1 and CPF-2 carrying the G42E Nio point mutation.

G42E allele into *TagRFP-cpf-2*. However, TagRFP::CPF-2^{G42E} did not alter CPF-2 protein abundance, nuclear localization, puncta formation, or colocalization with SYMK-1.

cpf-2 and *symk-1* Nio alleles also exhibit phenotypes associated with transcriptional termination and APA

The 3′ mRNA cleavage and polyadenylation complex is required for general RNA polymerase II mRNA cleavage and polyadenylation, transcriptional termination, and selection of specific DNA-encoded polyadenylation signal sequences. Mutation of *cpf-2* and *symk-1* could cause a Nio phenotype by disrupting these or other processes. Three pieces of data suggest that the Nio alleles do not disrupt global mRNA cleavage and/or polyadenylation at a significant level. First, total amounts of nucleic acid, which should be significantly reduced by inefficient polyadenylation, are not decreased in either *cpf-2(dr99)* or *symk-1(dr88)* (Supplementary Fig. 6). Second, polyA patterns and lengths for 4 highly expressed mRNAs are qualitatively similar between wild type, *cpf-2(dr99)*, or *symk-1(dr88)* (Supplementary Fig. 7). Third, induction of a heat shock inducible *hsp-16p::GFP* reporter, which shares the same *unc-54* 3′ UTR and polyA signal as the *gpdh-1p::GFP* reporter, is induced to wild-type levels in *cpf-2(dr99)* and *symk-1(dr88)* (Supplementary Fig. 8). Therefore, inhibition of *cpf-2* and *symk-1* does not generally block mRNA cleavage and polyadenylation.

To test if the Nio mutants alter transcriptional termination and/or recognition of specific polyA signal sequences, we asked if they could suppress phenotypes associated with either *lin-15(n765ts)* or *kin-20(ox423)*, 2 mutants that were previously shown to be suppressed by inhibition of the 3′ mRNA cleavage complex. Suppression of *lin-15(n765)* and *kin-20(ox423)* occurs specifically due to alterations in the ability of the 3′ mRNA cleavage complex to appropriately recognize DNA encoded APA signal sequences (Cui *et al.* 2008; LaBella *et al.* 2020). We found that the Nio allele of *cpf-2* completely suppressed the Muv phenotype *of lin-15(n765)* (Fig. 5a and b). Additionally, *symk-1* and *cpf-2* Nio alleles both suppressed the motility defects associated with the *kin-20* LOF mutation as well or better than the previously identified *kin-20* suppressor *cpsf-4(ox645)* (Fig. 5c and d). Together, these data show that *cpf-2* and *symk-1* Nio alleles both act to inhibit 3′ mRNA cleavage and can disrupt APA for these specific transcripts.

Inhibition of multiple components of the 3′ mRNA cleavage and polyadenylation complex also cause a Nio phenotype

If *cpf-2* and *symk-1* mutants cause a Nio phenotype due to inhibition of 3′ mRNA cleavage and selection of appropriate polyadenylation sequences, then inhibition of other components of this complex should also cause a Nio phenotype. To test this hypothesis, we examined if inhibition of other genes in the 3′ mRNA cleavage complex could also cause a Nio phenotype. Sixteen or

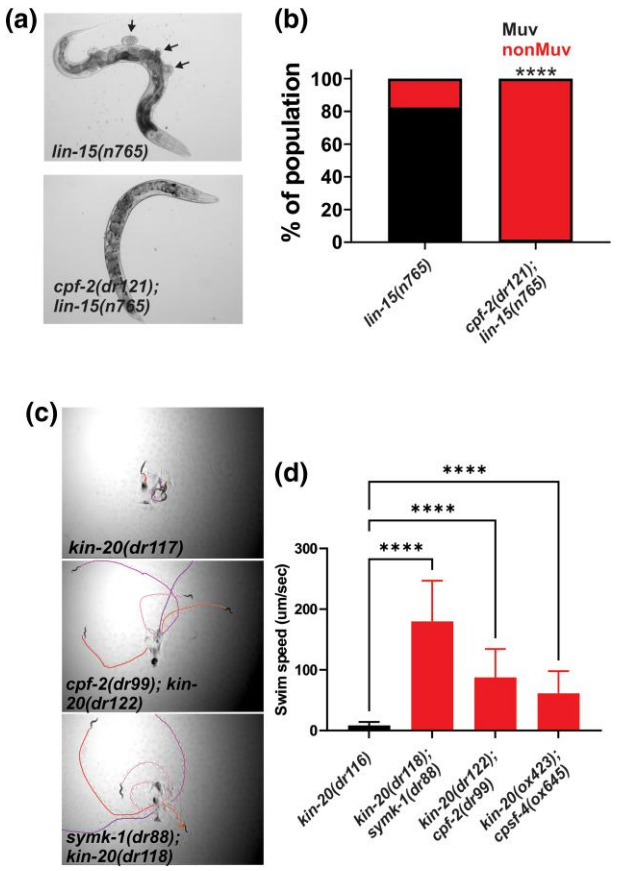

Fig. 5. *cpf-2* and *symk-1* suppress mutant phenotypes that depend on APA. a) Transmitted light images of *lin-15* or *lin-15; cpf-2* double mutants. Arrows in a point to multiple ectopic vulva which produces the multivulval or Muv phenotype. b) Quantification of the % of Muv and nonMuv animals from the indicated genotypes. ****$P < 0.0001$, Fishers exact test. $N = 102$ animals for *lin-15* and 120 animals for *cpf-2; lin-15*. c) Movement tracks for day 1 adult animals of the indicated genotypes. Each color represents and individual track. d) Swim speed for day 1 adult animals of the indicated genotypes. Data shown are mean ± SD for 10–24 animals per genotype. ****$P < 0.0001$; 1-way ANOVA with Dunn's multiple comparison test.

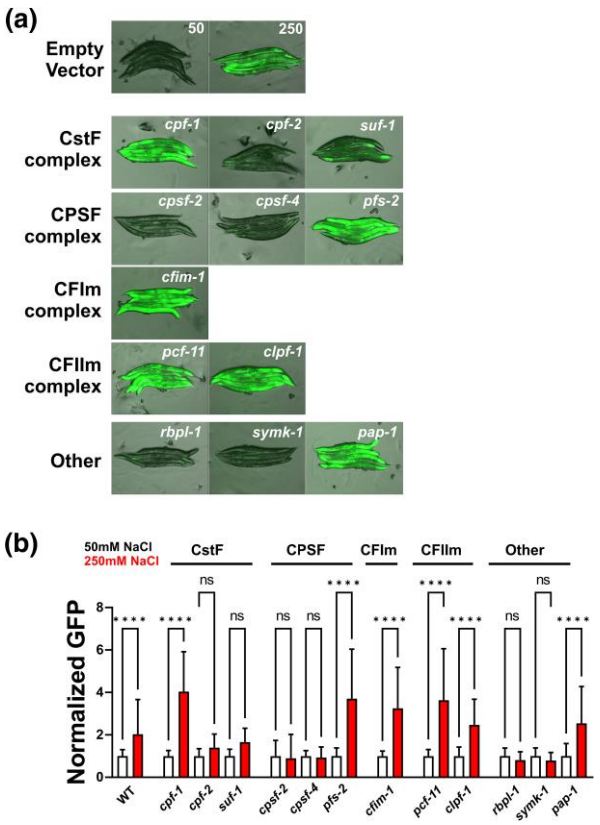

Fig. 6. Inhibition of a subset of APA complex genes causes a Nio phenotype. a) Merged GFP and transmitted light images of *drIs4* animals fed either *empty vector(RNAi)* or RNAi against the indicated APA complex genes. Only images for animals exposed to 250 mM NaCl for 24 h are shown for APA RNAi treatments. b) COPAS Biosort quantification of normalized GFP levels for each APA RNAi treatment following exposure to either 50 mM NaCl or 250 mM NaCl. Data shown are mean ± SD $N = 14$–61 animals per sample. ****$P < 0.0001$; ns $P > 0.05$; 1-way ANOVA with Šidák's multiple comparison test.

17 genes in the 3′ mRNA cleavage complex have clear orthologs in *C. elegans* (Steber et al. 2019). We obtained RNAi clones for 12/17 genes and performed post-developmental feeding-based RNAi in the *gpdh-1p::GFP* reporter strain. Following exposure to hypertonic stress, knockdown of *suf-1*, *cpsf-2*, *cpsf-4*, and *rbpl-1*, in addition to *cpf-2* and *symk-1* (6/12 tested), gave rise to a Nio phenotype (Fig. 6). Therefore, the Nio phenotype is not restricted to disruption of *cpf-2* and *symk-1* specifically but is caused by inhibition of multiple genes in the 3′ mRNA cleavage complex. Taken together, these data are consistent with a model in which inhibition of *cpf-2* and *symk-1* prevent hypertonic induction of *gpdh-1* due to the inability to recognize appropriate polyA signal sequences in a gene(s) required for activation of the hypertonic stress response.

Discussion

Phenotypes associated with loss of components of the 3′ mRNA cleavage complex, particularly at the organismal level, are poorly understood due to the fact that loss-of-function mutants in most members of this complex are lethal (Steber *et al.* 2019). One recent exception to this is in *C. elegans*, where unbiased genetic screens can isolate nonnull hypomorphic alleles of genes whose null phenotype is lethal. In this study, we discover a new role for this complex in the organismal response to hypertonic stress. Hypomorphic alleles of *cpf-2* and *symk-1* block hypertonic induction of *gpdh-1* and adaptation to hypertonicity through their post-developmental function in the intestine and hypodermis. How might this complex regulate hypertonicity-induced gene expression and hypertonic adaptation? One possibility is that the Nio defect may be due to generally inefficient polyadenylation which could reduce mRNA stability and inhibit the accumulation and translation of stress inducible mRNAs. Arguing against this is our finding that some inducible mRNAs and proteins, such as *nlp-29* and a heat shock induced gfp reporter, continue to be induced to normal levels in the *cpf-2* and *symk-1* mutants. This would be unlikely to occur if these mRNAs were inefficiently polyadenylated. Therefore, nonspecific defects in overall mRNA polyadenylation seems to be an unlikely explanation for the Nio phenotype of *cpf-2* and *symk-1*. Large-scale sequencing approaches mapping 3′ transcript termination sites and measuring individual transcript polyadenylation lengths will be needed to determine if these single observations extend to the genome-wide level.

Another possibility for how the 3′ mRNA cleavage complex regulates the hypertonic stress response is that APA of a specific target via regulation of the 3′ mRNA processing complex could be

required for appropriate execution of this physiological response. In this respect, 1 possible APA target is *gpdh-1*. However, evidence from thousands of RNAseq data sets does not reveal evidence for APA of *gpdh-1* itself (Steber *et al.* 2019), and genetic studies show that *gpdh-1* null alleles can still activate hypertonic adaptation (Urso *et al.* 2020). Instead, we hypothesize that 3′ mRNA cleavage could perform a similar function in the hypodermis and intestine to that in the neurons (LaBella *et al.* 2020), where it regulates polyA site usage of a signaling gene that is an essential signaling component of the hypertonic stress response. Alternatively, the function of the 3′ cleavage complex could regulate isoform switching for a suite of genes, such as extracellular matrix genes, whose collective function appears to be critical for the hypertonic stress response (Rohlfing *et al.* 2010, 2011; Dodd *et al.* 2018). Arguing against this second possibility is our observation that removal of the SYMK-1 protein in young adults after deposition of the ECM and immediately before exposure to hypertonicity is sufficient to block the hypertonic stress response. Defining the targets of 3′ mRNA cleavage complex in the *C. elegans* intestine and hypodermis using RNAseq and evaluating their functional roles in the Nio phenotype represent an important future direction and will help to further distinguish between these and other models.

Subcellular localization and protein–protein interactions play an important role in the function of the 3′ mRNA cleavage complex (Ruepp *et al.* 2011). Both CPF-2 and SYMK-1 are expressed in all observable somatic and germline nuclei in *C. elegans*. We found that hypertonic stress causes both proteins to undergo reorganization into subnuclear foci. The function of these foci is unclear. Recently, hyperosmotic stress was found to result in the phase separation of the APA factor CPSF6 (Jalihal *et al.* 2020), which leads to functional impairment of mRNA cleavage and polyadenylation. Whether or not this relocalization of the APA complex in *C. elegans* is related to its role in the Nio phenotype is not known. We found that introducing the G42E missense Nio allele into CPF-2 did not impact its ability to form subnuclear foci in response to hypertonicity or to colocalize with SYMK-1. Further studies will be needed to determine if hypertonic stress leads to functional impairment of transcriptional termination in *C. elegans* as it does in mammalian cells and whether or not large-scale termination events or target-specific APA contributes to the Nio phenotype.

In the same genetic screen that identified *cpf-2* and *symk-1*, we also identified null alleles in the O-GlcNAc transferase *ogt-1* (Urso *et al.* 2020). The discovery of all 3 genes in the same genetic screen suggests that they might act together as part of the same signaling complex. However, our data suggest that this may not be the case. First, *ogt-1* regulates *gpdh-1* expression via a post-transcriptional mechanism while *cpf-2* and *symk-1* function at the transcriptional level. Second, while both OGT-1 and CPF-2/SYMK-1 are nuclear proteins and form subnuclear foci in response to hypertonicity, these foci are spatially distinct. Despite these differences, there could be regulatory interactions between *ogt-1* and the 3′ cleavage complex. For example, a recent study shows that the TPR domain of mammalian OGT interacts with the 3′ cleavage complex components PCF11 (CFIIm complex) and CPSF1 (Stephen *et al.* 2021). Interestingly, it is the TPR domain, and not the catalytic activity, of OGT-1 that is required for the hypertonic stress response in *C. elegans* (Urso *et al.* 2020). Studies examining the role of *ogt-1* in the regulation of APA events will be needed to differentiate between these possibilities.

While the occurrence of APA has been known for several years, the regulatory mechanisms that determine which polyA site in a given gene will be utilized remain mysterious. Genetic approaches in organisms such as *C. elegans* provide a powerful opportunity to study this highly conserved and essential complex in many dynamic, tissue-specific settings. The tools and insights developed in this study will play a major role in future studies aimed at understanding the physiologically relevant targets of 3′ mRNA cleavage and APA in the hypertonic stress response and investigating the mechanisms that drive polyA site switching in response to dynamic environmental changes.

Data availability

Strains and plasmids are available upon request. The authors affirm that all data necessary for confirming the conclusions of the article are present within the article, figures, and tables.

Supplemental material available at GENETICS online.

Acknowledgments

We thank Maria Veroli Noguera, PhD (Pitt) and Robert G. Kalb, MD (Northwestern) for critical reading and review of the manuscript prior to submission and Marco Mangone, PhD (Arizona State University) for helpful discussions.

Conflict of interest

The author(s) declared no conflicts of interests.

Literature cited

Alt FW, Bothwell AL, Knapp M, Siden E, Mather E, Koshland M, Baltimore D. Synthesis of secreted and membrane-bound immunoglobulin mu heavy chains is directed by mRNAs that differ at their 3′ ends. Cell 1980;20(2):293–301. doi:10.1016/0092-8674(80)90615-7.

Ashley GE, Duong T, Levenson MT, Martinez MAQ, Johnson LC, Hibshman JD, Saeger HN, Palmisano NJ, Doonan R, Martinez-Mendez R, *et al.* An expanded auxin-inducible degron toolkit for *Caenorhabditis elegans*. Genetics 2021;217(3). doi:10.1093/genetics/iyab006.

Burkewitz K, Choe KP, Lee EC, Deonarine A, Strange K. Characterization of the proteostasis roles of glycerol accumulation, protein degradation and protein synthesis during osmotic stress in *C. elegans*. PLoS One 2012;7(3):e34153. doi:10.1371/journal.pone.0034153.

Calfon M, Zeng H, Urano F, Till JH, Hubbard SR, Harding HP, Clark SG, Ron D. IRE1 couples endoplasmic reticulum load to secretory capacity by processing the XBP-1 mRNA. Nature 2002;415(6867):92–96. doi:10.1038/415092a.

Chang J-W, Zhang W, Yeh H-S, Park M, Yao C, Shi Y, Kuang R, Yong J. An integrative model for alternative polyadenylation, IntMAP, delineates mTOR-modulated endoplasmic reticulum stress response. Nucleic Acids Res. 2018;46(12):5996–6008. doi:10.1093/nar/gky340.

Clerici M, Faini M, Aebersold R, Jinek M. Structural insights into the assembly and polyA signal recognition mechanism of the human CPSF complex. eLife 2017;6. doi:10.7554/eLife.33111.

Clerici M, Faini M, Muckenfuss LM, Aebersold R, Jinek M. Structural basis of AAUAAA polyadenylation signal recognition by the human CPSF complex. Nat Struct Mol Biol. 2018;25(2):135–138. doi:10.1038/s41594-017-0020-6.

Cui M, Allen MA, Larsen A, MacMorris M, Han M, Blumenthal T. Genes involved in pre-mRNA 3′-end formation and transcription termination revealed by a *lin-15* operon Muv suppressor screen.

Proc Natl Acad Sci U S A. 2008;105(43):16665–16670. doi:10.1073/pnas.0807104105.

Dodd W, Tang L, Lone J-C, Wimberly K, Wu C-W, Consalvo C, Wright JE, Pujol N, Choe KP. A damage sensor associated with the cuticle coordinates three core environmental stress responses in *Caenorhabditis elegans*. Genetics 2018;208(4):1467–1482. doi:10.1534/genetics.118.300827.

Ghanta KS, Mello CC. Melting dsDNA donor molecules greatly improves precision genome editing in *Caenorhabditis elegans*. Genetics 2020;216(3):643–650. doi:10.1534/genetics.120.303564.

Ha KCH, Blencowe BJ, Morris Q. QAPA: a new method for the systematic analysis of alternative polyadenylation from RNA-seq data. Genome Biol. 2018;19(1):45. doi:10.1186/s13059-018-1414-4.

Hollerer I, Curk T, Haase B, Benes V, Hauer C, Neu-Yilik G, Bhuvanagiri M, Hentze MW, Kulozik AE. The differential expression of alternatively polyadenylated transcripts is a common stress-induced response mechanism that modulates mammalian mRNA expression in a quantitative and qualitative fashion. RNA 2016;22(9):1441–1453. doi:10.1261/rna.055657.115.

Jalihal AP, Pitchiaya S, Xiao L, Bawa P, Jiang X, Bedi K, Parolia A, Cieslik M, Ljungman M, Chinnaiyan AM, *et al.* Multivalent proteins rapidly and reversibly phase-separate upon osmotic cell volume change. Mol Cell. 2020;79(6):978–990.e5. doi:10.1016/j.molcel.2020.08.004.

Kraynik SM, Gabanic A, Anthony SR, Kelley M, Paulding WR, Roessler A, McGuinness M, Tranter M. The stress-induced heat shock protein 70.3 expression is regulated by a dual-component mechanism involving alternative polyadenylation and HuR. Biochim Biophys Acta. 2015;1849(6):688–696. doi:10.1016/j.bbagrm.2015.02.004.

LaBella ML, Hujber EJ, Moore KA, Rawson RL, Merrill SA, Allaire PD, Ailion M, Hollien J, Bastiani MJ, Jorgensen EM. Casein kinase 1delta stabilizes mature axons by inhibiting transcription termination of ankyrin. Dev Cell. 2020;52(1):88–103.e18. doi:10.1016/j.devcel.2019.12.005.

Lamitina ST, Morrison R, Moeckel GW, Strange K. Adaptation of the nematode *Caenorhabditis elegans* to extreme osmotic stress. Am J Physiol Cell Physiol. 2004;286(4):C785–C791. doi:10.1152/ajpcell.00381.2003.

Lamitina T, Huang CG, Strange K. Genome-wide RNAi screening identifies protein damage as a regulator of osmoprotective gene expression. Proc Natl Acad Sci U S A. 2006;103(32):12173–12178. doi:10.1073/pnas.0602987103.

Mayr C, Bartel DP. Widespread shortening of 3′ UTRs by alternative cleavage and polyadenylation activates oncogenes in cancer cells. Cell 2009;138(4):673–684. doi:10.1016/j.cell.2009.06.016.

Pancevac C, Goldstone DC, Ramos A, Taylor IA. Structure of the Rna15 RRM-RNA complex reveals the molecular basis of GU specificity in transcriptional 3′-end processing factors. Nucleic Acids Res. 2010;38(9):3119–3132. doi:10.1093/nar/gkq002.

Pederiva C, Bohm S, Julner A, Farnebo M. Splicing controls the ubiquitin response during DNA double-strand break repair. Cell Death Differ. 2016;23(10):1648–1657. doi:10.1038/cdd.2016.58.

Pujol N, Cypowyj S, Ziegler K, Millet A, Astrain A, Goncharov A, Jin Y, Chisholm AD, Ewbank JJ. Distinct innate immune responses to infection and wounding in the *C. elegans* epidermis. Curr Biol. 2008;18(7):481–489. doi:10.1016/j.cub.2008.02.079.

Rohlfing AK, Miteva Y, Hannenhalli S, Lamitina T. Genetic and physiological activation of osmosensitive gene expression mimics transcriptional signatures of pathogen infection in *C. elegans*. PLoS One 2010;5(2):e9010. doi:10.1371/journal.pone.0009010.

Rohlfing AK, Miteva Y, Moronetti L, He L, Lamitina T. The *Caenorhabditis elegans* mucin-like protein OSM-8 negatively regulates osmosensitive physiology via the transmembrane protein PTR-23. PLoS Genet. 2011;7(1):e1001267. doi:10.1371/journal.pgen.1001267.

Ruepp MD, Schweingruber C, Kleinschmidt N, Schumperli D. Interactions of CstF-64, CstF-77, and Symplekin: implications on localisation and function. Mol Biol Cell. 2011;22(1):91–104. doi:10.1091/mbc.e10-06-0543.

Shanbhag NM, Rafalska-Metcalf IU, Balane-Bolivar C, Janicki SM, Greenberg RA. ATM-dependent chromatin changes silence transcription in cis to DNA double-strand breaks. Cell 2010;141(6):970–981. doi:10.1016/j.cell.2010.04.038.

Shi Y, Di Giammartino DC, Taylor D, Sarkeshik A, Rice WJ, Yates JR, Frank J, Manley JL. Molecular architecture of the human pre-mRNA 3′ processing complex. Mol Cell 2009;33(3):365–376. doi:10.1016/j.molcel.2008.12.028.

Steber HS, Gallante C, O'Brien S, Chiu PL, Mangone M. The *C. elegans* 3′ UTRome v2 resource for studying mRNA cleavage and polyadenylation, 3′-UTR biology, and miRNA targeting. Genome Res. 2019;29(12):2104–2116. doi:10.1101/gr.254839.119.

Stephen HM, Praissman JL, Wells L. Generation of an interactome for the tetratricopeptide repeat domain of O-GlcNAc transferase indicates a role for the enzyme in intellectual disability. J Proteome Res. 2021;20(2):1229–1242. doi:10.1021/acs.jproteome.0c00604.

Subramanian A, Hall M, Hou H, Mufteev M, Yu B, Yuki KE, Nishimura H, Sathaseevan A, Lant B, Zhai B, *et al.* Alternative polyadenylation is a determinant of oncogenic Ras function. Sci Adv. 2021;7-(51):eabh0562. doi:10.1126/sciadv.abh0562.

Tranter M, Helsley RN, Paulding WR, McGuinness M, Brokamp C, Haar L, Liu Y, Ren X, Jones WK. Coordinated post-transcriptional regulation of Hsp70.3 gene expression by microRNA and alternative polyadenylation. J Biol Chem. 2011;286(34):29828–29837. doi:10.1074/jbc.M111.221796.

Urso SJ, Comly M, Hanover JA, Lamitina T. The O-GlcNAc transferase OGT is a conserved and essential regulator of the cellular and organismal response to hypertonic stress. PLoS Genet. 2020;16(10):e1008821. doi:10.1371/journal.pgen.1008821.

Wang R, Nambiar R, Zheng D, Tian B. Polya_DB 3 catalogs cleavage and polyadenylation sites identified by deep sequencing in multiple genomes. Nucleic Acids Res. 2018;46(D1):D315–D319. doi:10.1093/nar/gkx1000.

Wimberly K, Choe KP. An extracellular matrix damage sensor signals through membrane-associated kinase DRL-1 to mediate cytoprotective responses in *Caenorhabditis elegans*. Genetics. 2022;220(3). doi:10.1093/genetics/iyab217.

Yuan F, Hankey W, Wagner EJ, Li W, Wang Q. Alternative polyadenylation of mRNA and its role in cancer. Genes Dis. 2021;8(1):61–72. doi:10.1016/j.gendis.2019.10.011.

Zheng D, Wang R, Ding Q, Wang T, Xie B, Wei L, Zhong Z, Tian B. Cellular stress alters 3′ UTR landscape through alternative polyadenylation and isoform-specific degradation. Nat Commun. 2018;9(1):2268. doi:10.1038/s41467-018-04730-7.

Editor: G. Seydoux